Racecar Longitudinal Control in Unknown and Highly-Varying Driving Conditions

Salvatore Pedone and Adriano Fagiolini

***Abstract*—This paper focuses on racecar longitudinal control with highly-varying driving conditions. The main factors affecting the dynamic behavior of a vehicle, including aerodynamic forces, wheel rolling resistance, traction force resulting from changing tire-road interaction as well as the occurrence of sudden wind gusts or the presence of persistent winds, are considered and assumed to have unknown models. By exploiting the theory on delayed input-state observers and using measurement data about the vehicle and wheel speeds, a dynamic filter that allows the online reconstruction of the above-mentioned unknown time-varying quantities is derived. Moreover, by exploiting the notion of effective tire radius, a reduced-degree-of-freedom model for the longitudinal vehicle dynamics is obtained, which is independent of the traction force and that enables, when used with the observer filter described above, an accurate speed control compensating for the resistance forces. One appealing feature of the proposed estimation and control method is that it requires no model information about such forces, for which, at the state-of-the-art, only heuristic approximations to be a-priori identified are available. Its effectiveness is shown via the simulation of scenarios where the car is required to execute aggressive maneuvers and the asphalt road surface abruptly changes from dry to wet, snowy, and icy. The evaluation also reveals that the proposed estimation technique outperforms standard solutions even in the presence of measurement noise.**

***Index Terms*—Self-driving, autonomous Vehicles, racecars, input-state estimation.**

I. Introduction

In THE near future, a great number of automotive applications will become possible [1], by leveraging on the availability of denser and faster communication networks that will soon be enabled by the 5G technology [2]. Via the Vehicle-to-Everything (V2X) architecture [3], all actors of future transport systems (vehicles, passengers, and pedestrians) [4], [5] will be able to cooperatively plan and optimize their travel experience [6], according to faster [7], more efficient [8], secure [9], and safer [10]–[12] protocols. They will be able to share evidence of possible hazards, including unexpected traffic jams in tunnels, road damages, anomalous behavior of human drivers and autonomous pilots [13], [14], thus improving the overall safety of passengers and pedestrians [15]. In this scenario, the race towards (electric) vehicles with full self-driving capacity has just begun [16]–[19]. However, several obstacles have to be overcome before this technology goes mainstream to the market [20], including an infrastructure modernization [21], [22], the definition of legislations addressing moral and legal issues [23], [24], and the achievement of stronger guarantees on the ability of an autonomous vehicle to detect and react to uncertainties caused by unexpected changes in the driving conditions.

The two major sources of uncertainty when modeling a vehicle's dynamics are related to the traction force and the presence of external disturbance [25]. The traction force is proportional to the instantaneous friction coefficient, whose value can be computed only using heuristic functions, experimentally identified [26], [27], that require the knowledge of the type of road (dry, wet, snowy, and icy). In a realistic scenario, in which the road surface may change unexpectedly, the road type detection can be done by using visual data, but the accuracy of this process is affected by light conditions and the asphalt reflection property. External disturbance is due to sudden wind gusts, aerodynamic drag, and rolling resistance. Modeling persistent or rapidly changing winds, such as those occurring when exiting from a tunnel, driving on viaducts and overpasses [28], or as a result of the interaction with another approaching vehicle, is not easy. Direct measurement of the wind speed can be done by using anemometer sensors, based on pitot probes, which however are less accurate at lower speed, require altitude-dependent calibration, must be installed far enough from the vehicle to catch only laminar airflow, and introduce further costs. Consequently, even though the aerodynamic drag force can be accurately modeled, its direct estimation may be imprecise as it needs the information about the vehicle's speed relative to the wind velocity. The rolling resistance force is also known approximately, and its identification is vehicle-specific and requires so-called coast-down tests.

In order to obtain safe and performant control of a vehicle's motion, one can either use robust control techniques, such as sliding mode control [29], or estimate the unknown quantities by using dynamic input-state observers. Regarding the second approach, it has been recently shown that online estimation of tire-road interaction forces can be obtained if a full model, including tires, wheels, and vehicle dynamics, is considered [30]. Observers-based solutions can estimate the instantaneous maximum available power [31] and even allow prompt intervention of drivers upon risk detection [32]. The standard way of estimating a vehicle's state is undoubtedly by using Kalman filters [33], [34], which are optimal estimators when the vehicle is moving

Manuscript received May 23, 2020; revised August 8, 2020; accepted August 21, 2020. Date of publication September 9, 2020; date of current version November 12, 2020. This work has been partially funded by MIUR under project POC R&I 2014-2020 "Dottorati innovativi a caratterizzazione industriale". The review of the article was coordinated by Dr. D. Cao. *(Corresponding author: Adriano Fagiolini.)*

The authors are with the Department of Engineering, University of Palermo,, Italy (e-mail: salvatore.pedone@unipa.it; adriano.fagiolini@unipa.it).

Digital Object Identifier 10.1109/TVT.2020.3023059

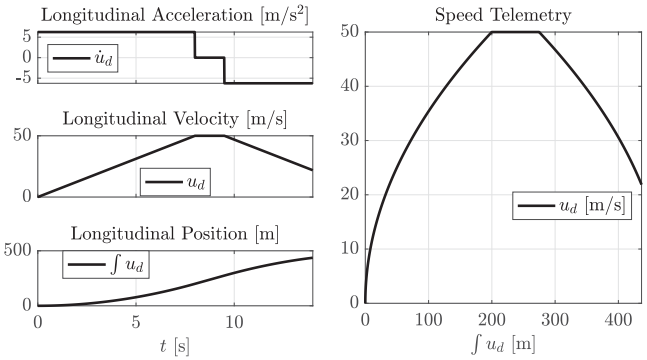

Fig. 1. Example of a telemetry plot depicting an aggressive maneuver in which a racecar accelerates from 0 to 180 km/h (50 m/s) in 8 seconds with a constant acceleration of 6.25 m/s^2, then moves at a constant high speed, and finally decelerates with opposite acceleration rate.

at a constant speed for almost all time. This optimality is lost if the vehicle performs aggressive driving maneuvers, made of sequences of acceleration and deceleration phases, when the nonlinear traction force is uncertain, or when the external disturbance is far from being a Gaussian noise signal. The estimation of the traction force and the other external disturbance signals named above can be obtained by using Extended Kalman Filters (EKF). These filters provide good results, but they require adding new states to the observers and accurate modeling of their dynamics [35]–[37]. Discontinuous changes in the friction coefficient can be handled with adaptive estimators, thanks to the introduction of a parameter update law [38].

Within this context, this paper addresses the longitudinal speed control problem for a racecar under unknown and highly-varying driving conditions. The aim is to provide the controlled vehicle with the capacity to asymptotically track an aggressive maneuver, i.e. a trajectory with a constant high-speed plateau [39], preceded and followed by fast acceleration/deceleration phases (Fig. 1). The problem is attacked by first deriving a novel estimator, which is built upon input-reconstruction theory [40] and which reconstructs the uncertain and unknown time-varying quantities affecting the vehicle dynamics, then obtaining a convenient reduced-degree-of-freedom model, and finally achieving a feedback control for the sought tracking.

Contribution. The contribution of this paper is at least threefold. First, the paper presents an input-state observer that uses only vehicle's and wheel speed measures and that allows estimating the current traction force, the resultant of the resistance forces, and the so-called effective tire radius. An appealing feature of the observer – and indeed its main novelty – is its independence from the knowledge of the actual time-varying traction model, the wind model, and the vehicle-specific rolling and aerodynamic coefficients. Such an independence is inherited from the decoupling of state and input reconstruction that is achieved by using so-called Unknown Input Observers (UIO) [40]. The observer is computationally light, i.e. it consists of a linear dynamic system of the same order of the vehicle dynamics and a linear mapping reconstructing the unknown inputs, it is directly implementable on embedded hardware, and it is very fast. Contrarily to this solution, an EKF-based approach requires adding additional states to the estimator, needs tuning the entries of the covariance matrices, possesses no convergence guarantees, and leads to a much slower estimation convergence. Even a solution using windspeed measurement would require converting the speed to the corresponding wind force, which involves knowing the exact vehicle-dependent aerodynamic coefficients and which is not needed in the presented approach. As a second contribution, under the assumption of small values for the slip ratio variable (later defined), a reduced-degree-of-freedom model for the vehicle's dynamics is derived, which is independent of the traction force. Based on this model and by using data estimated by the input-state observer, the paper describes a feedback control law that allows the asymptotic tracking of aggressive maneuvers, while maintaining the slip ratio below a desired threshold, irrespectively of the presence of external disturbance and abrupt changes in the traction force. Thirdly, the effectiveness and performance of the overall solution are shown through a series of simulations, carried out first with a nominal model, then adding system and measurement noise, and subsequently by using the Vehicle Dynamics Blockset. This last tool emulates more realistic driving conditions and allows showing the robustness of the proposed approach also to model uncertainties. Finally, real-time execution of the approach is proved via the implementation on a real Raspberry PI hardware.

II. System Modeling and Problem Statement

The purpose of this section is to present the dynamical model of a racecar and to formalize the estimation and control problems that are addressed in this work.

A. Dynamic Model of the Vehicle

Consider a racecar with rear traction traveling along a flat and straight road. Under the common assumptions of having tires with identical geometric and inertial characteristics and traction that can be generated instantaneously, the dynamic behavior of the car is described by the so-called bicycle model [25]. Referring to such a model, by denoting with ω the speed of the virtual rear wheel and with u the longitudinal velocity of the vehicle, the following dynamic equations can be used

$$\begin{aligned} I_\omega \dot{\omega} &= T - R_\omega(\dot{u})\, F_t(\omega, u, \dot{u})\,, \\ m\,\dot{u} &= F_t(\omega, u, \dot{u}) - F_a(u) - F_r(u)\,, \end{aligned} \tag{1}$$

where I_ω is the wheel's inertia along the rotation axis, m is the vehicle mass, T is the input driving torque, R_ω is the so-called effective tire radius, F_t is the rear traction force, F_a is the aerodynamic drag force, and F_r is the total rolling resistance force summing up the effects at all tires.

Though the model appears to be very compact, its complexity is actually encoded in every single term composing the dynamic expressions in Eq. 1, whose analysis reveals that the model is still in implicit form, thereby hindering the underlying estimation and control problems. More precisely, the effective tire radius R_ω relates the rotational wheel velocity ω to the linear longitudinal wheel velocity as it moves through the contact patch of the tire with the ground [41]. It can be shown that R_ω can be

expressed according to the formula:

$$R_\omega = \frac{\sin(\arccos(R_d/R))}{\arccos(R_d/R)} R\,, \tag{2}$$

where R and R_d are the tire's undeformed and dynamic radii, respectively, the latter of which is obtained as follows:

$$R_d = R - \frac{F_z(\dot{u})}{K_t}, \tag{3}$$

with F_z the vertical force acting on the rear tire and K_t its stiffness along the vertical direction. In turn, the vertical force F_z is obtained as a static term, depending on the geometry of the car and being present in conditions of constant longitudinal speed, and a dynamic one directly proportional to the longitudinal acceleration $\dot{u}$ and expressing the normal load transfer between front and rear axles during acceleration and braking phases. In particular, it holds [25]

$$F_z = \frac{m}{l}\left(g\, a_1 + h\, \dot{u}\right)\,, \tag{4}$$

with l is the wheelbase, i.e. the distance between the rear and front axles, a_1 is the distance between the front axle and the vehicle's center of mass, and h is the height of the center of gravity from to the road. Based on this reasoning the effective tire radius is in the general case a function of the instantaneous longitudinal acceleration, i.e. $R_\omega = R_\omega(\dot{u})$.

Moreover, the rear traction force F_t is highly dependent on many factors, among which are the characteristics of the road and the type of interaction between the tire and the road asphalt. At the state-of-the-art only heuristic expressions are available, which consist of static models providing the instantaneous traction force F_t as a function of the wheel speed ω, longitudinal velocity u and acceleration $\dot{u}$, and other parameters to be ad-hoc identified (see e.g. [42]). For the sake of generality, the dynamics considered in Eq. 1 does not refer to any of such models, and as such the sought solution will do, while to evaluate the proposed solution the so-called Burckhardt's and Pacejka's formulas will be used later in Sec. V-C. Similar reasoning holds for the expressions of the aerodynamic drag force F_a and rolling resistance force F_r. Here, it is also assumed that the vehicle's pitching motion is limited and can occur only at the beginning of the acceleration or braking phase. This allows neglecting the effect of the suspensions on the vehicle's dynamic behavior, which is present only during short initial transients.

Furthermore, it can be assumed that the wheel's and longitudinal vehicle's speeds are available. Indeed, in modern cars, measurement of the wheel speed ω can be obtained from the Antilock Brake System (ABS), while that of the vehicle's longitudinal speed u can be provided by speedometer sensors, whose accuracy can be improved by fusion with GPS speed data [43] and even LiDar measurement [44]. More precisely, speedometers must provide by regulation a measured speed that is always equal or greater than the real one, and never bigger than the 110% of it, plus 4 km/h [45]. In practice, digital speedometers have a lower upper bound of uncertainty of 2/3%. GPS speed accuracy can vary and be affected by e.g. weather conditions, obstruction by surrounding building, and sudden direction changes, but it increases with the vehicle speed [46], as the ratio of positional error to positional change is lower. It has been estimated, with a typical GPS equipment, that the average measurement error decreases from 4.55% at around 20 km/h down to 1.57% at 50 km/h. Combination of these sensors' data allows then even better performance.

Within this setting, the present work addresses the following two problems:

Problem 1 (Estimation of Racecar Unknown Inputs): Given the racecar's dynamic model in Eq. 1, design a dynamic estimator reconstructing the current traction force F_t, the overall resistance force $F_l = F_a(u) - F_r(u)$, and the effective tire radius R_ω, by using only knowledge of the input driving torque T and measurement of ω and u.

Problem 2 (Tracking Control with Disturbance Compensation): Given a racecar system described by the dynamic model in Eq. 1, find a control law for the input driving torque T that allows asymptotic tracking of a desired longitudinal velocity $u_d(t)$ and that is independent of the traction and resistance force model. By using information from the estimator solving the problem above, the sought controller must be able to compensate for the effect of disturbance and model uncertainties.

III. Estimation of Resistance Force, Traction Force, and Effective Tire Radius

This section first recalls the theory on delayed unknown input observers from [40] and then describes the design of an observer allowing the estimation of the actual driving torque T, resistance force F_l, and effective radius R_ω.

A. Delayed UIO—Theoretical Framework

UIOs allow simultaneous state estimation and unknown input reconstruction by exploiting the equivalence between linear system's invertibility and unknown input observability [47], [48]. Consider a linear discrete-time system of the form

$$\begin{aligned} X_{k+1} &= A\,X_k + B\,U_k\,,\\ Y_k &= C\,X_k + D\,U_k\,, \end{aligned} \tag{5}$$

where $X_k \in \mathbb{R}^n$ is a state vector, $U_k \in \mathbb{R}^m$ contains the unknown inputs, $Y_k \in \mathbb{R}^p$ is an output vector, A, B, C, and D are suitable matrices. Given a time delay L, the history of the system's output $\mathbb{Y}_k^L = (Y_k^T, \cdots, Y_{k+L}^T)^T$, can be obtained as

$$\mathbb{Y}_k^L = O^L X_k + \mathbb{H}^L\, U_k^L\,, \tag{6}$$

where $\mathbb{U}_k^L = (U_k^T, \cdots, U_{k+L}^T)^T$ is the input history, and $O^L = (C^T, (CA)^T, (CA^2)^T, \cdots, (CA^{L-1})^T)^T = \\ = (C^T, (O^{L-1}A)^T)^T\,,$

and

$$\mathbb{H}^L = \begin{pmatrix} D & 0 \\ O^{L-1}B & \mathbb{H}^{L-1} \end{pmatrix}. \tag{7}$$

are the *L-step observability and invertibility matrices*, respectively. A discrete-time linear UIO is given by

$$\begin{aligned} \hat{X}_{k+1} &= E\,\hat{X}_k + F\,\mathbb{Y}_k^L\,,\\ \hat{U}_k &= G\begin{pmatrix} \hat{X}_{k+1} - A\,\hat{X}_k \\ Y_k - C\,\hat{X}_k \end{pmatrix}, \end{aligned} \tag{8}$$

where E and F are observer matrices of suitable dimensions, being designed such that $\hat{X}_k \to X_k$ and $\hat{U}_k \to U_k$, and where $G = (B^T, D^T)^{T\,\dagger}$ is an input decoupling matrix, with full column rank, and $P^\dagger$ is the pseudo-inverse of a matrix P.

The UIO existence conditions are stated in the following:

Proposition 1 (Existence of delayed UIO): Given a linear dynamic system of the form in Eq. 5, an L-step delayed UIO described by Eq. 8 exists if, and only if, there exist two matrices E and F satisfying the conditions:

1) E is Schur, i.e. all its eigenvalues lay within the unit circle of the complex plane,
2) $E = A - F\,O^L$, and
3) $F\,\mathbb{H}^L = (B, 0_{n\times Lm})$.

Proof: Direct computation of the dynamics of the state estimation error yields

$$\begin{aligned} e_{k+1} &= \hat{X}_{k+1} - X_{k+1} \\ &= E\,\hat{X}_k + F\,\mathbb{Y}_k^L - A\,X_k - B\,U_k \\ &= E\,e_k + F\,\mathbb{Y}_k^L + (E - A)\,X_k - B\,U_k \\ &= E\,e_k + (E - A + F\,O^L)\,X_k \\ &\quad + F\,\mathbb{H}^L\,U_k^L - B\,U_k, \end{aligned}$$

which, under the theorem's assumptions, reduces to $e_{k+1} = E\,e_k$, thereby guaranteeing convergence for every unknown input signal U_k and every initial state e_0.

The solvability of the third condition of Prop. 1 is ensured by the system's invertibility, as anticipated above, which is recalled here for the reader's convenience:

Proposition 2 (System Invertibility): A linear dynamic system with state form as in Eq. 5, with state vector $X_k \in \mathbb{R}^n$ and $U_k \in \mathbb{R}^m$, is *invertible with delay* L if, and only if, the condition

$$\text{rank}\left(\mathbb{H}^L\right) = m + \text{rank}\left(\mathbb{H}^{L-1}\right) \tag{9}$$

is satisfied for some $L \leqslant n$, where $\text{rank}(\mathbb{H}^{-1}) = 0$ by definition.

Moreover, the design procedure allowing the computation of the sought matrices E, F, and G can be found in [40], [49], and it is shortly presented below. More precisely, to be able to reconstruct the system state X_k, it is necessary to determine matrices E and F so that E is Schur, E has the structure described in the second condition and involving F, and finally, F satisfies the third condition. It is then natural to proceed in the reverse direction, by starting from the computation of F. The third condition of Prop. 1 requires that matrix $F \in \mathbb{R}^{n\times Lp}$ is in the left nullspace of the last Lm columns of the L-step invertibility matrix $\mathbb{H}^L$. Under the iterative rule expressed in Eq. 7, this requirement translates in asking that the last Lm columns of F be in the left nullspace of the matrix

$$H_2^L = \begin{pmatrix} 0 \\ \mathbb{H}^{L-1} \end{pmatrix}.$$

Having then denoted with $\bar{N}^{L-1}$ a basis of the left nullspace of $\mathbb{H}^{L-1}$, the matrix

$$\begin{pmatrix} I_p & 0 \\ 0 & \bar{N}^{L-1} \end{pmatrix}$$

is a basis of the left nullspace of H_2^L. This means that any linearly independent combinations of the rows of $\bar{N}^L$ satisfy, by construction, the relation:

$$W \begin{pmatrix} I_p & 0 \\ 0 & \bar{N}^{L-1} \end{pmatrix} \mathbb{H}^L = W \begin{pmatrix} D & 0 \\ \bar{N}^{L-1} O^{L-1}\,B & 0 \end{pmatrix},$$

where W is a free invertible matrix collecting all the combination coefficients. Moreover, Eq. 9 implies that the rank of matrix $\begin{pmatrix} D \\ \bar{N}^{L-1} O^{L-1}\,B \end{pmatrix}$ is m, and thus it is possible to choose $W = (W_1^T, W_2^T)^T$ so that its bottom m rows W_2 and top remaining ones W_1 are a left inverse and in the left nullspace of the above matrix, respectively. Namely, the matrix

$$N = W \begin{pmatrix} I_p & 0 \\ 0 & \bar{N}^{L-1} \end{pmatrix} \tag{10}$$

is such that

$$N\,\mathbb{H}^L = \begin{pmatrix} 0 & 0 \\ I_m & 0 \end{pmatrix}.$$

This reasoning suggests that F can be found by factorizing it as $F = (F_1, F_2)N$, which allows obtaining

$$F\,\mathbb{H}^L = (F_1, F_2) \begin{pmatrix} 0 & 0 \\ I_m & 0 \end{pmatrix} = (B, 0),$$

from which it is obvious that $F_2 = B$ and F_1 is a free matrix. The second condition of Prop. 1 then becomes $E = A - (F_1, B)S$ with

$$S = \begin{pmatrix} S_1 \\ S_2 \end{pmatrix} = NO^L, \tag{11}$$

where S_2 is composed of the bottom m rows of S. Matrix E is rewritten as

$$E = A - B\,S_2 - F_1\,S_1, \tag{12}$$

where F_1 is a free matrix which is finally chosen to ensure that all its eigenvalues are within the unit circle.

Finally, the unknown inputs can be reconstructed by rearranging the state form equations as:

$$\begin{pmatrix} X_{k+1} - A\,X_k \\ Y_k - C\,X_k \end{pmatrix} = \begin{pmatrix} B \\ D \end{pmatrix} U_k, \tag{13}$$

which, under the assumption that $(B^T, D^T)^T$ is full column rank, can be inverted via a matrix G such that

$$G \begin{pmatrix} B \\ D \end{pmatrix} = I_m. \tag{14}$$

Indeed, by left-multiplying both members of Eq. 13 by G and replacing X_k with its best available estimate $\hat{X}_k$, we finally obtain the last relation in Eq. 8.

B. Design of the Proposed Estimator for the Racecar Model

In order to estimate the sought unknown inputs affecting the racecar, it is first necessary to obtain a time-discretized version of the model described in Eq. 1. To this purpose, by introducing a sampling time δ and approximating all time derivatives by

their first-order Euler approximations, the following discrete-time system is obtained:

$$\begin{aligned} \omega_{k+1} &= \omega_k - \frac{\delta}{I_\omega} R_{\omega,k}\, F_{t,k} + \frac{\delta}{I_\omega} T_k\,, \\ u_{k+1} &= u_k + \frac{\delta}{m}\left(F_{t,k} - F_{a,k} - F_{r,k}\right)\,, \end{aligned} \tag{15}$$

where $\omega_k = \omega(k\delta)$, $u_k = u(k\delta)$, $R_{\omega,k} = R_\omega(k\delta)$, $F_{t,k} = F_t(k\delta)$, $F_{a,k} = F_a(k\delta)$, $F_{r,k} = F_r(k\delta)$, $T_k = T(k\delta)$, and k is a discrete time step. Therefore, one can define the current state sample vector as $X_k = (\omega_k, u_k)^T$.

As a second step, in order to apply the methodology described above, it is instrumental to consider all forces and torque acting on the system as unknown inputs, and thus defined the unknown input sample vector as

$$U_k = \begin{pmatrix} U_{1,k} \\ U_{2,k} \end{pmatrix} = \begin{pmatrix} T_k - R_{\omega,k}\, F_{t,k} \\ F_{t,k} - F_{l,k} \end{pmatrix}\,, \tag{16}$$

where $F_{l,k} = F_{a,k} + F_{r,k}$ is the total resistance force. More precisely, this choice is motivated by the necessity to ensure the satisfaction of the invertibility condition of Prop. 2. Indeed the below obtained input matrix is full column rank. Assume also that both state variables are available as system outputs, which, as clarified above, can be read by encoders mounted on the wheels and a speedometer measuring the longitudinal speed. Accordingly, Eq. 15 can be rewritten as

$$X_{k+1} = A\, X_k + B\, U_k\,, \tag{17}$$

where the remaining matrices are given by

$$A = I_{2\times 2}\,,\; B = \begin{pmatrix} \frac{\delta}{I_\omega} & 0 \\ 0 & \frac{\delta}{m} \end{pmatrix}\,,\; C = I_{2\times 2}\,,\; D = 0_{2\times 2}\,. \tag{18}$$

Given the above discrete-time state form of the racecar's dynamic model, the following result can be stated, which solves Prob. 1:

Theorem 1 (Traction and Resistance Forces Estimator): Given a discrete-time state form as in Eq. 5, a UIO system estimating the state of the system and its unknown inputs is described by the state-form in Eq. 8, where the delay step is $L = 1$ and

$$\begin{aligned} E &= \begin{pmatrix} \lambda_\omega & 0 \\ 0 & \lambda_u \end{pmatrix}\,,\quad F = \left(\begin{array}{cc|cc} -\lambda_\omega & 0 & \frac{\delta}{I_\omega} & 0 \\ 0 & -\lambda_u & 0 & \frac{\delta}{m} \end{array}\right)\,, \\ G &= \begin{pmatrix} \frac{I_\omega}{\delta} & 0 & 0 & 0 \\ 0 & \frac{m}{\delta} & 0 & 0 \end{pmatrix}\,, \end{aligned} \tag{19}$$

where λ_ω and λ_u are free constants that can be chosen so as to allocate the estimation error eigenvalues. Moreover, given the estimated unknown inputs $\hat{U}_k = (\hat{U}_{1,k}, \hat{U}_{2,k})^T$, best-effort estimates of the dynamic tire radius, the traction force and total resistance forces, respectively, are given by the following formulas:

$$\hat{R}_{d,k} = R - \frac{\hat{F}_{z,k}}{K_t} = R - \frac{mga}{lK_t} - \frac{h}{lK_t}\hat{U}_{2,k}\,, \tag{20}$$

and

$$\begin{pmatrix} \hat{F}_t \\ \hat{F}_l \end{pmatrix} = \begin{pmatrix} \dfrac{T - \hat{U}_{1,k}}{\hat{R}_{\omega,k}} \\ \dfrac{T - \hat{U}_{1,k}}{\hat{R}_{\omega,k}} - \hat{U}_{2,k} \end{pmatrix}\,. \tag{21}$$

Finally, a best-effort estimate of the effective tire radius $\hat{R}_{\omega,k}$ is obtained by using Eq. 2 and the estimate $\hat{R}_{d,k}$ from Eq. 20.

Proof: The proof proceeds by determining first the required step delay L, then the estimators matrices, and finally proving the unknown input reconstruction formulas.

1) Delay Computation: As a first step, one has to determine the required delay step L. According to Prop. 2, the sought delay can be found by searching the smallest integer L satisfying condition 9. This shows that $L = 1$ since the invertibility matrices in 0 and 1 steps, respectively, are $\mathbb{H}^0 = D = 0_{2\times 2}$,

$$\mathbb{H}^1 = \begin{pmatrix} D & 0 \\ CB & D \end{pmatrix} = \begin{pmatrix} 0 & 0 & 0 & 0 \\ 0 & 0 & 0 & 0 \\ \frac{\delta}{I_\omega} & 0 & 0 & 0 \\ 0 & \frac{\delta}{m} & 0 & 0 \end{pmatrix}\,.$$ As the first two columns of $\mathbb{H}^1$ are linearly independent while the other ones are null, or equivalently the last two columns are linearly independent while the first two are null, it holds $\text{rank}(\mathbb{H}^1) - \text{rank}(\mathbb{H}^0) = 2 - 0 = 2 = m$, which is the number of unknown inputs.

2) Design of the Estimator: We can now proceed to design the one-step delayed observer for system of Eq. 17 and 18. Given that $m = 2$ and $L = 1$, the third condition of Prop. 1 requires that matrix F satisfies the equation $F\,\mathbb{H}^1 = (B, 0_{2\times 2})$, which implies that F has to be in the left nullspace of the last $Lm = 2$ columns of the one-step invertibility matrix $\mathbb{H}^1$. Since $\mathbb{H}^0$ is null, a basis of its left nullspace can be described by matrix $\bar{N}^0 = I_2$. According to the reasoning expressed in subsection III-B, matrix W has to be found such that $W \begin{pmatrix} 0 & 0 \\ 0 & 0 \\ \frac{\delta}{I_\omega} & 0 \\ 0 & \frac{\delta}{m} \end{pmatrix} = \begin{pmatrix} 0 & 0 \\ 0 & 0 \\ 1 & 0 \\ 0 & 1 \end{pmatrix}$. A possible choice of W is thus $W = \begin{pmatrix} 1 & 0 & 0 & 0 \\ 0 & 1 & 0 & 0 \\ 0 & 0 & \frac{I_\omega}{\delta} & 0 \\ 0 & 0 & 0 & \frac{m}{\delta} \end{pmatrix}$ and correspondingly $N = W \begin{pmatrix} I_2 & 0 \\ 0 & \bar{N}^0 \end{pmatrix} = W$. Moreover, by using the 1-step observability matrix $O^1 = \begin{pmatrix} 1 & 0 & 1 & 0 \\ 0 & 1 & 0 & 1 \end{pmatrix}^T$ one can obtain from the relation $S = NO^1$ (see Eq. 11) the following sub-matrices: $S_1 = I_2\,,\quad S_2 = \begin{pmatrix} \frac{I_\omega}{\delta} & 0 \\ 0 & \frac{m}{\delta} \end{pmatrix}$. According to Eq. 12, the estimation error dynamics is given by $E = A - B \begin{pmatrix} \frac{I_\omega}{\delta} & 0 \\ 0 & \frac{m}{\delta} \end{pmatrix} - F_1 = \begin{pmatrix} 0 & 0 \\ 0 & 0 \end{pmatrix} - F_1$. Since all eigenvalue of E are already inside the unit circle (and indeed in the origin), matrix F_1 can be null. More generally, if the eigenvalues are required to be placed at

λ_ω and λ_u, the output injection matrix F_1 can be chosen as in Eq. 19. Finally, having guaranteed by the choice of the unknown inputs, that the matrix $(B^T, D^T)^T$ is full column rank, it is possible to find a matrix G that satisfies Eq. 14. For the system in consideration, this relation is $G \begin{pmatrix} B \\ D \end{pmatrix} = G \begin{pmatrix} \frac{\delta}{I_\omega} & 0 \\ 0 & \frac{\delta}{m} \\ 0 & 0 \\ 0 & 0 \end{pmatrix} = I_2$, whose solution can be computed via the pseudo-inverse and gives the expression reported in Eq. 19.

3) Refinement of the Effective Tire Radius Estimate: Once the current value of the unknown input $\hat{U}_k$ has been reconstructed, one can observe that its second component $\hat{U}_{2,k}$ represents the total force acting along the vehicle's longitudinal direction (cf. the second equation of the model in Eq. 1). As such, an estimate $\hat{\dot{u}}_k$ of the instantaneous longitudinal acceleration $\dot{u}$ of the racecar can be obtained by dividing for its mass m, i.e. as

$$\hat{\dot{u}}_k = \frac{\hat{U}_{2,k}}{m}. \tag{22}$$

This enables first obtaining a more accurate, best-effort estimate $\hat{F}_{z,k}$ of the tire's normal (vertical) load F_z via Eq. 4, that is $\hat{F}_{z,k} = \frac{m}{l}(g\,a + h\frac{\hat{U}_{2,k}}{m}) = \frac{a}{l}mg + \frac{h}{l}\hat{U}_{2,k}$, which can be used to reach the best-effort dynamic tire radius estimate $\hat{R}_{d,k}$ described in Eq. 20, and finally the corresponding one for the effective tire radius $\hat{R}_{\omega,k}$, which is more accurate than the a-priori value $R_{\omega,0}$.

4) Computation of the Traction and Resistance Forces: After having reconstructed the current effective tire radius $\hat{R}_{\omega,k}$, based on the fact that the wheel drive torque T is known, the traction and resistance forces can be algebraically derived by solving the following system in Eq. 16 with respect to them, that is $\begin{pmatrix} \hat{U}_{1,k} \\ \hat{U}_{2,k} \end{pmatrix} = \begin{pmatrix} T - \hat{R}_{\omega,k}\,\hat{F}_t \\ \hat{F}_t - \hat{F}_l \end{pmatrix}$ which yields the formulas described in Eq. 21.

IV. The Proposed Speed Control With Active Drag Compensation

The scope of this section is to reformulate the dynamical model of a racecar, in a way that makes it independent of the traction force F_t, and to describe a nonlinear speed controller actively compensating the estimated resistance forces. More in detail, the challenge in controlling the vehicle's longitudinal dynamics stems in coping with the highly unknown and time-varying functions describing e.g. the traction F_t and resistance F_l forces. Such a function may dynamically vary depending on the tire and asphalt interaction, temperature, etc. These variations can adversely affect the vehicle's motion stability, especially in racecars when e.g. an opponent car in the wake entails a significant drop in the aerodynamic load. Therefore, it is mandatory to develop, as we do below, a control law that is independent of the mathematical formulas describing such functions and that uses only reconstructed data obtained e.g. by the above proposed UIO.

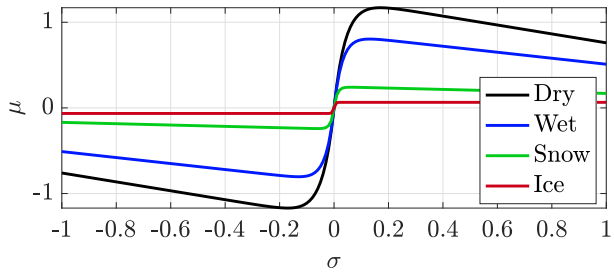

Fig. 2. Characteristics of the friction coefficient μ for various nominal types of tire/road surface [26]. Maximum values are attained for slip ratios in the range [0.06, 0.17]. The instantaneous traction force F_t is related to the friction coefficient via the formula in Eq. 39.

A. Dynamic Model Reformulation

To achieve independence on the highly unknown traction force F_t, it is convenient to rewrite the system's model described in Eq. 1 to make this term disappear and reach an explicit form of the state dynamics. To this aim, first, solve the first expression in Eq. 1 for F_t, which yields: $F_t(\omega, u, \dot{u}) = \frac{T - I_\omega\,\dot{\omega}}{R_\omega(\dot{u})}$, and substitute it in the second expression of Eq. 1, leading to

$$m\,\dot{u} = \frac{T - I_\omega\,\dot{\omega}}{R_\omega(\dot{u})} - F_a(u) - F_r(u)\,. \tag{23}$$

Moreover, it is known that the traction force F_t depends on the slip ratio σ, a quantity that will be defined later in Eq. 38. It is worth noticing that F_t reaches its maximum for slip ratio values that range between 0.06 and 0.17, depending on the tire/road surface, and then decreases for larger values [26] (Fig. 2). It is therefore desirable to control a car's motion, while maintaining σ small or practically null, which becomes particularly advantageous in the context of racecars as the obtained traction force is maximized. Under this assumption, it can be shown that the effective tire radius R_ω coincides with the time-varying coefficient instantaneously translating the wheel speed ω to that of the vehicle's longitudinal velocity u, via the ratio [50]:

$$R_\omega = \frac{u}{\omega}. \tag{24}$$

Rewriting this equation as $u = R_\omega\,\omega$ and computing its time-derivative allow obtaining $\dot{u} = \dot{R}_\omega(\dot{u})\,\omega + R_\omega(\dot{u})\,\dot{\omega}$ whose solution for the wheel acceleration $\dot{\omega}$ is

$$\dot{\omega} = \frac{\dot{u} - \dot{R}_\omega(\dot{u})\,\omega}{R_\omega(\dot{u})}, \tag{25}$$

which, substituted in Eq. 23, allows achieving the expression:

$$\frac{mR_\omega^2(\dot{u}) + I_\omega}{R_\omega^2(\dot{u})}\dot{u} - \frac{\dot{R}_\omega(\dot{u})}{R_\omega^2(\dot{u})}I_\omega\,\omega - \frac{T}{R_\omega(\dot{u})} = -F_a(u) - F_r(u)\,. \tag{26}$$

While the exact differential system, described in the above equation, is still implicit, due to the nonlinear dependency on $\dot{u}$, which does not allow its factorisation as a multiplicative term, a nonlinear yet simplified model can be obtained by observing the following. First, it is worth noticing that the racecar is nominally

intended to be operated at regimes with piecewise-constant (even null) longitudinal accelerations, i.e. with $\ddot{u} = 0$ for almost all times. Therefore, by this assumption, the effective tire radius $R_\omega(\dot{u})$ becomes exactly constant and its derivative identically null. Indeed, it holds: $\dot{R}_\omega(\dot{u}) = \dfrac{\partial R_\omega(\dot{u})}{\partial \dot{u}}\,\ddot{u} = 0$. Therefore, indicating, as above, the total resistance force as $F_l(u) = F_a(u) + F_r(u)$, the following traction-force independent model of the longitudinal dynamics of a racecar is obtained:

$$\left(m + \frac{I_\omega}{R_\omega^2(\dot{u})}\right)\dot{u} = \frac{T}{R_\omega(\dot{u})} - F_l(u)\,. \tag{27}$$

Remark 1: Note that, under the above assumptions, the wheel's dynamics in Eq. 25 also simplifies as $\dot{\omega} = \dot{u}/R_{\omega,0}$, thus solving the problem of trajectory tracking for u, also ensures tracking of the corresponding wheel tracking. Therefore, the stability of the above-obtained model guarantees that of the wheel's dynamics, namely, the system dynamics is reduced to a one degree of freedom.

B. Control System Design

The above reformulation of the dynamic model, from Eq. 1 to Eq. 27, enables a great simplification in the derivation of a controller, as it is shown in the following result, which solves Prob. 2:

Theorem 2: Given a racecar described by the dynamic model in Eq. 27, a desired trajectory $u_d(t)$ for the car's longitudinal velocity, and a desired convergence speed $\kappa > 0$ for the tracking error $e_u = u - u_d$, the best-effort feedback and feed-forward control law described by

$$T = \frac{m\hat{R}_{\omega,k}^2 + I_\omega}{\hat{R}_{\omega,k}}\left(\dot{u}_d - \frac{\kappa}{2}(u - u_d)\right) + \hat{R}_{\omega,k}\,\hat{F}_l(u)\,, \tag{28}$$

where $\hat{R}_{\omega,k}$ and $\hat{F}_l$ are the estimated effective tire radius and resistance forces obtained by means of Eq. 20 and Eq. 21, respectively, ensures exponential asymptotic tracking of u_d and requires no information about the traction force F_t.

Proof: Let us first introduce the positive quantity $m^*(\dot{u}) = m + \frac{I_\omega}{R_\omega^2(\dot{u})}$. In order to design a control law allowing the tracking of a desired velocity u_d, or equivalently, ensuring that the tracking error e_u exponentially converges to zero, consider the Lyapunov control function $V(e_u) = \frac{1}{2}m^*(\dot{u})\,e_u^2$, which is positive definite around $e_u = 0$ and whose directional derivative is $\dot{V} = e_u\,m^*(\dot{u})\,\dot{e}_u$. By plugging the expression of the system's dynamics described in Eq. 27 into the quantity $m^*(\dot{u})\,e_u = m^*(\dot{u})\,\dot{u} - m^*(\dot{u})\,\dot{u}_d$, and then substituting the result into the above expression of the Lyapunov's directional derivative yields

$$\dot{V} = \; e_u\left(\frac{T}{R_\omega(\dot{u})} - F_l(u) - m^*(\dot{u})\,\dot{u}_d\right)\,. \tag{29}$$

To guarantee the asymptotic stability of the equilibrium point $e_u = 0$, $\dot{V}$ must be negative definite. To obtain also that a desired convergence speed of κ is achieved, one can impose the expression in Eq. 29 to be equal to

$$\dot{V} = -\kappa\,V = e_u\left(-\frac{\kappa}{2}m^*(\dot{u})\,e_u\right)\,, \tag{30}$$

which leads to the condition $\dfrac{T}{R_\omega(\dot{u})} - F_l(u) - m^*(\dot{u})\,\dot{u}_d = -\frac{\kappa}{2}m^*(\dot{u})\,e_u$ and, then, to the following formula for the driving torque: $T = m^*(\dot{u})R_\omega(\dot{u})(\dot{u}_d - \dfrac{\kappa}{2}(u - u_d)) + R_\omega(\dot{u})\,F_l(u)\,.$ Under the assumption that the UIO described in Th. 1 has converged, one can replace the unknown quantities R_ω and F_l with the estimated ones, $\hat{R}_{\omega,k}$ and $\hat{F}_l$, respectively, and thus obtain the best-effort control described in Eq. 28.

Finally, with the above choice of T, the solution of the differential equation described by the first two members of Eq. 30 is $V(t) = e^{-\kappa t}\,V(0)$, with $V(0) = \frac{1}{2}m^*(\dot{u}(0))\,e_u^2(0)$, that exponentially converges to zero with speed κ. This result also concludes the proof.

Remark 2 (Maximum Deliverable Torque): During acceleration or deceleration phases, a longitudinal wheel's slip ratio σ, which will be defined later in Eq. 38 of Sec. V), always occurs. The reduced-degree-of-freedom model of Eq. 27 has been found under the hypothesis of a null slip, but it remains valid also for small values of such a variable. To ensure that the absolute value of the slip ratio is kept within a threshold $\bar{\sigma}$, the driving torque function in Eq. 28 is replaced by the formula

$$T = \frac{I_\omega}{\hat{R}_{\omega,k}}\hat{\dot{u}} + \hat{R}_{\omega,k}\left(\hat{F}_{l,k} + |\hat{F}_{t,k} - \hat{F}_{l,k}|\,\mathrm{sign}(\sigma)\right)\,, \tag{31}$$

whenever the condition $|\sigma| \geq \bar{\sigma}$ is detected.

To explain this choice, it is first convenient to find a differential equation for the slip ratio variable σ. During an acceleration phase with $u_d > u$, the (positive) slip ratio variable is $\sigma = 1 - u/(\omega R_\omega)$ (cf. the first expression of Eq. 38). Rewriting its definition as $u - (1-\sigma)wR_\omega = 0$ and differentiating it with respect to time yields $\dot{u} + \dot{\sigma}\,\omega\,R_\omega - (1-\sigma)\,\dot{\omega}\,R_\omega = 0$. Solving this last equation for $\dot{\sigma}$ and using the equivalence $\dot{u} = R_\omega\,\dot{\omega}$ (valid for small σ) gives

$$\dot{\sigma} = -\frac{\dot{u}}{u}\,\sigma\,. \tag{32}$$

During a deceleration phase ($u_d < u$ and $\sigma < 0$), the slip ratio is defined as $\sigma = \omega R_\omega/u - 1$ (cf. the second expression of Eq. 38). With a similar reasoning as above, one obtains $\dot{\sigma}\,u + (1+\sigma)\,\dot{u} - \dot{\omega}\,R_\omega = 0$, whose solution for $\dot{\sigma}$ gives again the formula in Eq. 32.

Moreover, for a vehicle moving forward ($u > 0$) with a slip ratio having reached a maximum allowed value, i.e. $\sigma \geq \bar{\sigma} > 0$, it must be ensured that the condition $\dot{\sigma} < 0$ holds, which is satisfied if $\dot{u} > 0$. A possible choice for the driving torque T ensuring the above condition is $T = \frac{I_\omega}{R_\omega}\dot{u} + R_\omega(F_l + |F_t - F_l|)$, which, plugged into the vehicle's longitudinal dynamics of Eq. 27, yields $(m + \frac{I_\omega}{R_\omega^2})\dot{u} = \frac{I_\omega}{R_\omega^2}\dot{u} + |F_t - F_l|$, and hence

$$m\,\dot{u} = |F_t - F_l| \geq 0\,. \tag{33}$$

The simultaneous satisfaction of $\dot{\sigma} \leq 0$ and $\dot{u} \geq 0$ implies that the car is controlled so that to reduce the slip ratio σ while

TABLE I
INERTIAL AND GEOMETRIC PARAMETERS OF A RACECAR AS IN THE ROBORACE CHALLENGE [17]

Parameters	Value	Unit
Vehicle's Mass, m	1350	[Kg]
Vehicle's Inertia Moment, J	1150	[Kg $\cdot$ m^2]
Center of gravity height from ground, h	0.5	[m]
Front wheelbase, a_1	1.51	[m]
Rear wheelbase, a_2	1.288	[m]
Wheelbase, l	2.798	[m]
Effective tire Radius (Static), $R_{\omega,0}$	0.5	[m]
Wheel's Inertial Moment, I_ω	1.125	[Kg $\cdot$ m^2]

still increasing (or at least not decreasing) its speed u toward the desired value u_d. Conversely, if the slip ratio has reached a minimum allowed value ($\sigma \leq -\bar{\sigma} < 0$), it must occur that $\dot{\sigma} > 0$ and thus that $\dot{u} < 0$. For this case, the choice $T = \frac{I_\omega}{R_\omega}\dot{u} + R_\omega(F_l - |F_t - F_l|)$ allows obtaining the longitudinal vehicle's speed dynamics

$$m\,\dot{u} = -|F_t - F_l| \leq 0\,. \tag{34}$$

The simultaneous conditions $\dot{\sigma} \geq 0$ and $\dot{u} \leq 0$ enables to maintain small the slip ratio while the car's velocity is reduced toward the desired u_d. It is straightforward to see that the above two choices for T can be combined together, thereby leading to Eq. 31, where the unknown quantities have been replaced with their corresponding estimates. One can notice that, the condition $F_t = F_l$, for which $\dot{\sigma} = \dot{u} = 0$, can only happen for specific combinations of the tire/road surface and the vehicle's aerodynamic coefficients, and in fact it may only be present for few instants. Therefore, the inequalities in Eq. 33 and Eq. 34 are practically always satisfied in the strict sense, and so are the ones involving $\dot{\sigma}$.

V. SIMULATION, VALIDATION, AND PERFORMANCE COMPARISON

This section validates the effectiveness of the proposed estimation and control approach, and it compares it to the performance achieved by using an EKF. The evaluation and comparison are carried out via simulations realized in Matlab/Simulink environment. Numerical data used to develop the simulations refer to the setting of a *Robocar*, one of the self-driving racecars participating in the Roborace Challenge [17]. Geometric and inertial parameters of the car are summarized in Table I.

A. Numerical Implementation of the Proposed UIO

Referring to the numerical values reported in Table I and choosing a sampling time $\delta = 10^{-3}$ s the effective tire radius corresponding to null acceleration $\dot{u} = 0$ is $R_{\omega,0} = 0.5\,[m]$ and the matrices of the racecar model in Eq. 18 becomes $A = I_2\,,\ B = \begin{pmatrix} 8.89 \cdot 10^{-3} & 0 \\ 0 & 7 \cdot 10^{-7} \end{pmatrix}$. Moreover, by choosing the observer eigenvalues $\lambda_\omega = -0.02$ and $\lambda_u = 0.02$ to be small but not coincident, so that to reduce the numerical sensitivity of the filter, the UIO matrices from Th. 1 becomes

$$E = \begin{pmatrix} -0.02 & 0 \\ 0 & 0.02 \end{pmatrix},$$

$$F = \begin{pmatrix} -0.02 & 0 & 8.89 \cdot 10^{-3} & 0 \\ 0 & 0.02 & 0 & 7 \cdot 10^{-7} \end{pmatrix},$$

$$G = \begin{pmatrix} 1.1248 \cdot 10^2 & 0 & 0\ 0 \\ 0 & 1.429 \cdot 10^6 & 0\ 0 \end{pmatrix}$$

B. Design of the Comparative EKF for Unknown Input Estimation

Let us briefly recall in the following the theoretical framework of an EKF (cf. e.g. [51], [52]) and show how this can be used for estimating the unknown inputs of our system. Consider a generic discrete-time process governed by a stochastic difference equation of the form

$$\begin{aligned} Z_{k+1} &= f(Z_k, U_k, W_k)\,, \\ Y_k &= h(Z_k, V_k)\,, \end{aligned} \tag{35}$$

where Z_k is a state vector, U_k are known inputs, Y_k is the output vector, W_k and V_k are the process and measurement noise, respectively, f and h are possibly nonlinear functions describing the system dynamic and output maps. W_k and V_k are assumed to be independent random processes with white Gaussian distributions and time-varying covariance matrices denoted as Q_k and R_k, respectively.

As it is known, an EKF for a dynamic system of the form in Eq. 35 consists of a two-phase algorithm during which an a-priori estimate $\hat{Z}_k^-$ of the system state Z_k and an a-posteriori one $\hat{Z}_k$ are computed. More precisely, $\hat{Z}_k^-$ is calculated during the *state prediction phase* based on knowledge of the process before the arrival of the k-th measurement Y_k; afterward, the *state update phase* realizes a feedback mechanism incorporating the new measures in the a-priori estimate $\hat{Z}_k^-$ so to obtain the improved a-posteriori one $\hat{Z}_k$. The a-priori and a-posteriori estimation processes are characterized by the following covariance matrices: $\begin{aligned} P_k^- &= E[(Z_k - \hat{Z}_k^-)(Z_k - \hat{Z}_k^-)^T]\,, \\ P_k &= E[(Z_k - \hat{Z}_K)(Z_k - \hat{Z}_k)^T]\,, \end{aligned}$ where $E[\cdot]$ is the expectation value operator. We also recall that, compared to a linear Kalman filter, an EKF differs in the fact that the matrices involved in the Riccati equations are obtained by linearization of the nonlinear state equations in 35, around the state estimated during the previous step. The EKF operation is summarized in Algorithm 1 [53].

Moreover, given a dynamic system in the form of Eq. 35, a common approach to use EKF for allowing, as in the scope of the present work, both state and unknown input reconstruction, requires to enhance the system state with additional variables representing such unknown inputs. To model the evolution of these newly added variables, the random walk process dynamics is assumed [54]. In the present case of the racecar, the traction force F_t and resistance force F_l are added as variables and the system state becomes $Z_k = (\omega_k, u_k, F_{t,k}, F_{l,k})^T$, and, starting from the two difference relations in Eq. 15, its corresponding

Algorithm 1: Modified EKF for Racecar Unknown Input Estimation.

loop
- $\hat{Z}^-_{k+1} = f(\hat{Z}_k, U_k)$ ▷Compute the a-priori estimate
- $\hat{Y}_k = h(\hat{Z}^-_k)$ ▷Compute predicted measures
- $A_k = \dfrac{\partial f(Z_k, U_k)}{\partial Z_k}_{Z_k=\hat{Z}^-_{k+1}}$ ▷Compute dynamic map Jacobian
- $H_k = \dfrac{\partial h(Z_k)}{\partial Z_k}_{Z_k=\hat{Z}^-_{k+1}}$ ▷Compute dynamic map Jacobian
- $P^-_{k+1} = A_k\, P_k\, A_k^T + Q_k$ ▷Compute the a-priori error covariance
- **wait untill** Y_k is available
- $K_k = P^-_{k+1} H_k^T\, (H_k\, P^-_{k+1} H_k^T + R_k)^{-1}$ ▷Update Kalman gain
- $\hat{Z}_k = \hat{Z}^-_k + K_k(Y_k - \hat{Y}_k)$ ▷Update the a-posteriori estimate
- $P_{k+1} = (I - K_k\, H_k) P^-_k$ ▷Update the a-posteriori error covariance

end loop

dynamics becomes

$$\begin{aligned} \omega_{k+1} &= \omega_k + (T_k - R_{\omega,k}\, F_{t,k})\, \delta / I_\omega + w_{1,k}\,, \\ u_{k+1} &= u_k + (F_{t,k} - F_{l,k})\, \delta / m + w_{2,k}\,, \\ F_{t,k+1} &= F_{t,k} + w_{3,k}\,, \\ F_{l,k+1} &= F_{l,k} + w_{4,k}\,. \end{aligned} \tag{36}$$

Analogously to the setting of the UIO, the quantities available for measurement are the wheel speed ω_k and longitudinal vehicle's velocity u_k. Then, the output vector is obtained as

$$Y_k = \begin{pmatrix} 1\,0\,0\,0 \\ 0\,1\,0\,0 \end{pmatrix} Z_k + V_k\,, \tag{37}$$

where $V_k = (v_{1,k}, v_{2,k})^T$ is the output noise. The Jacobian matrices of the dynamic and output maps from 36 are

$$A_k = \begin{pmatrix} 1\,0 & -R_{\omega,k}\delta/I_\omega & 0 \\ 0\,1 & \delta/m & -\delta/m \\ 0\,0 & 1 & 0 \\ 0\,0 & 0 & 1 \end{pmatrix}, \quad H_k = \begin{pmatrix} 1\,0\,0\,0 \\ 0\,1\,0\,0 \end{pmatrix}.$$

Under similar reasoning as for the UIO in Sec. III-B, once the last two entries of the augmented state vector Z_k, representing estimates of the traction $F_{t,k}$ and resistance $F_{l,k}$ forces, respectively, have been reconstructed by the EKF, one can obtain the instantaneous longitudinal acceleration as $\hat{\dot{u}} = \dfrac{\hat{F}_{t,k} - \hat{F}_{l,k}}{m} = \dfrac{\hat{Z}_{3,k} - \hat{Z}_{4,k}}{m}$ by inverting the second relation of Eq. 1. Plugging this result in the load weight formula in Eq. 4 allows obtaining $\hat{F}_z = \frac{m}{l}(g\, a_1 + h\, \hat{\dot{u}}) = m\, g\, \frac{a_1}{l} + \frac{h}{l}(\hat{Z}_{3,k} - \hat{Z}_{4,k})$, which finally allows the reconstruction of the current effective tire radius, $\hat{R}_{\omega,k}$ from Eq. 2 and 3.

Finally, referring to the numerical value listed in Table I, the Jacobian matrix of the dynamic map becomes

$$A_k = \begin{pmatrix} 1\,0 & -\hat{R}_{\omega,k} \cdot 1.125 \cdot 10^{-3} & 0 \\ 0\,1 & 8.89 \cdot 10^{-3} & -8.89 \cdot 10^{-3} \\ 0\,0 & 1 & 0 \\ 0\,0 & 0 & 1 \end{pmatrix}.$$

C. Simulation Results

To validate and assess the effectiveness of the proposed solution, the estimation and control approaches presented here have been tested in simulation within the Matlab/Simulink environment. A Robocar model characterized by the parameters listed in I has been used. Two scenarios have been considered in which the racecar is required to track a series of aggressive maneuvers as described below.

1) First Simulation Scenario: The first scenario includes the following components:

Traction force model F_t: A well-known formula that used to describe the effect of interaction between a car's tire and the road asphalt and, more precisely, that allows obtaining the instantaneous traction force F_t as a nonlinear function of the vehicle's velocity u, wheel speed ω, and terrain properties, is the so-called Burckhardt tire model [26]. Having denoted with

$$\sigma(\omega, u) = \begin{cases} 1 - \dfrac{u}{\omega R_\omega}, & \text{if } \omega R_\omega > u \text{ (acceleration phase)}\,, \\ \dfrac{\omega R_\omega}{u} - 1 & \text{if } \omega R_\omega < u \text{ (braking phase)}\,, \end{cases} \tag{38}$$

the *longitudinal slip ratio*, the instantaneous *friction coefficient* can be described as $\mu(\sigma) = \mu_1(1 - e^{-\mu_2 |\sigma|}) - \mu_3 |\sigma|$, where μ_1 represents its maximum value, μ_2 defines its curve shape, and μ_3 indicates the difference between the coefficient's maximum value (μ_1) and that obtained at full slip ratio with $\sigma = 1$. The values of the constants μ_i depend on the instantaneous kind of tire-asphalt interaction and thus may with time as the car moves. Then, the traction force F_t can be computed as

$$F_t(\omega, u, \dot{u}) = \mu(\sigma)\, F_z(\dot{u})\,, \tag{39}$$

where F_z is the normal component of the rear wheel load, i.e. the portion of the vehicle's weight applied to the tire, which can be obtained via Eq. 4. For the simulated scenario, the considered kinds of tire-asphalt interactions are dry-dry, dry-wet, and dry-ice. The corresponding values for all μ_i can be found e.g. in [42], [55], [56], which were obtained by curve-fitting experimentally obtained data. According to Remark 2, a conservative yet not too stringent value for the slip ratio threshold $\bar{\sigma}$ has been chosen equal to 0.08, so as to maintain the reduced-degree-of-freedom model valid.

Resistance force model F_l: The rolling resistance force F_r is known to be a function of the total normal load $F_z(\dot{u})$ acting on the tire, which in turn depends on the vehicle's velocity. However, as shown in [50], it is possible to approximate such a function by using a fourth-order Taylor expansion of the longitudinal velocity u, i.e. $F_r(u) = r_0 + r_1\, u + r_2\, u^4$, where the constants r_i depend on the tire characteristics. As in [50], we have assumed that the racecar is provided with radial tire

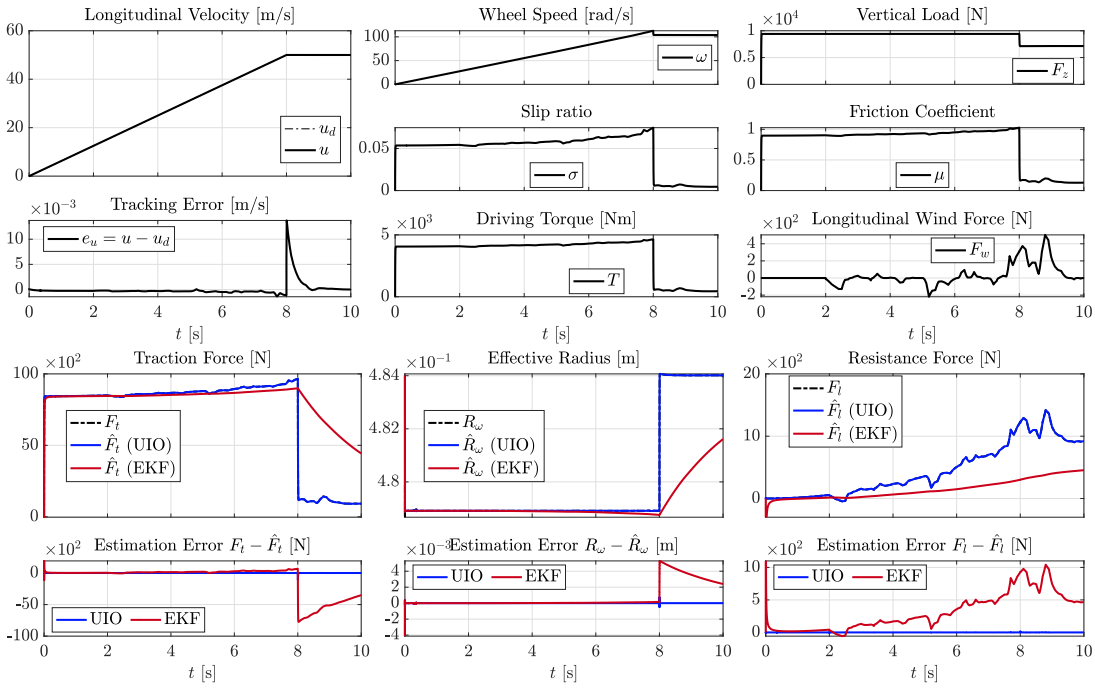

Fig. 3. Scenario #1.1 (Dry Asphalt): Typical simulation run where the racecar travels along a straight and dry road and is required to track a longitudinal velocity profile $u_d(t)$, when a sudden wind gust hits the vehicle at $t = 2$. The UIO is effectively able to reconstruct the unknown inputs and that the controller can track the desired trajectory and rapidly compensate for the effect of all resistances and disturbances.

types for which typical values of these constants are used: $r_0 = 9.91 \cdot 10^{-3}, r_1 = 1.95 \cdot 10^{-5}$, and $r_2 = 1.76 \cdot 10^{-9}$. Moreover, the aerodynamic drag force F_a is obtained according to the well-known relationship: $F_a(u) = \frac{1}{2}\,\rho\, S\, C_x\, (u + u_w)^2$, where ρ is the air density, S the frontal surface of the vehicle, C_x the aerodynamic drag coefficient along the longitudinal axis and u_w is the wind speed. Simulations address the case where the racecar travels at sea-level, and hence the air density is around $\rho = 1.225$ Kg/m^3, and assume the following values for the car parameters: $S = 2$ m^2 and $C_x = 0.3$. In the nominal cases, the resistance force is then given by $F_l(u) = F_r + F_a = r_0 + r_1\, u + \frac{1}{2}\,\rho\, S\, C_x\, u^2 + r_2\, u^4$.

Wind Gusts: Simulations aim also at testing the ability of the proposed estimation and control solution to cope with disturbance due to wind gusts. Such unknown inputs are described via the Dryden turbulence model [57], according to which the linear and angular speed components of a continuous gust can be represented as spatially-varying stochastic processes. In particular, the model specifies for the longitudinal component of the gust velocity the following power spectral density $\Phi_u = \frac{2\sigma_u^2 L_u}{\pi V} \frac{V^2}{V^2 + L_u^2 \omega_g^2}$ where L_u is the turbulence scale length, V is the airspeed, σ_u is the turbulence intensity, and ω_g is the temporal frequency of the gust.

To generate a turbulence signal that has a similar frequency spectrum as Dryden power spectral density the Dryden continuous filter is used, derived from the square roots of the Dryden power spectrum. This filter can be expressed through the following transfer function:

$$H_u(s) = \sigma_u \sqrt{\frac{2L_u}{\pi V}} \frac{1}{1 + \frac{L_u}{V} s} \tag{40}$$

We have discretized a length of the turbulence scale for a low altitude region, as described extensively in [57], having chosen: a height from sea level $h = 6\,m$, an airspeed $V = 50 \frac{m}{s}$ and a level of turbulence described by $W_{20} = 15\,Knots$. Finally, to simulate the magnitude of the wind force, the value of the wind speed coming from the Dryden model is added to that of the longitudinal speed in the discretization of the aerodynamic drag force. The Matlab implementation of the wind gust model can be found in [58].

Within this scenario, three typical simulation runs have been conducted. The first simulation reproduces a situation in which the racecar is assumed to be traveling along a straight and dry road and is required to track a longitudinal velocity profile $u_d(t)$, when a sudden wind gust instantaneously hits the vehicle. Fig. 3 shows the dynamic behavior of the closed-loop system, using the proposed UIO from Th. 1 and the controller proposed in Th. 2. The simulation shows that the UIO is effectively able to reconstruct the unknown inputs and that the controller can track the desired trajectory and rapidly compensate for the effect of the disturbances. Fig. 3 also show how the proposed UIO performs better than the Kalman-based approach, while also not requiring any information about the unknown inputs. More specifically, the unknown input estimates obtained by the UIO always converge faster than those of the EKF. This becomes more apparent when the car reaches the cruise speed at $t = 8$ seconds and the traction force F_t is immediately reduced as it only needs to compensate for the dissipative forces. This slower behavior of the EKF is explained as follows. In the EKF, the unknown inputs are variables of the estimator with a random-walk dynamics. The entries of the covariance matrix P_k associated with such variables converges to appropriate small quantities, thus reducing with time the adaptability of the filter to

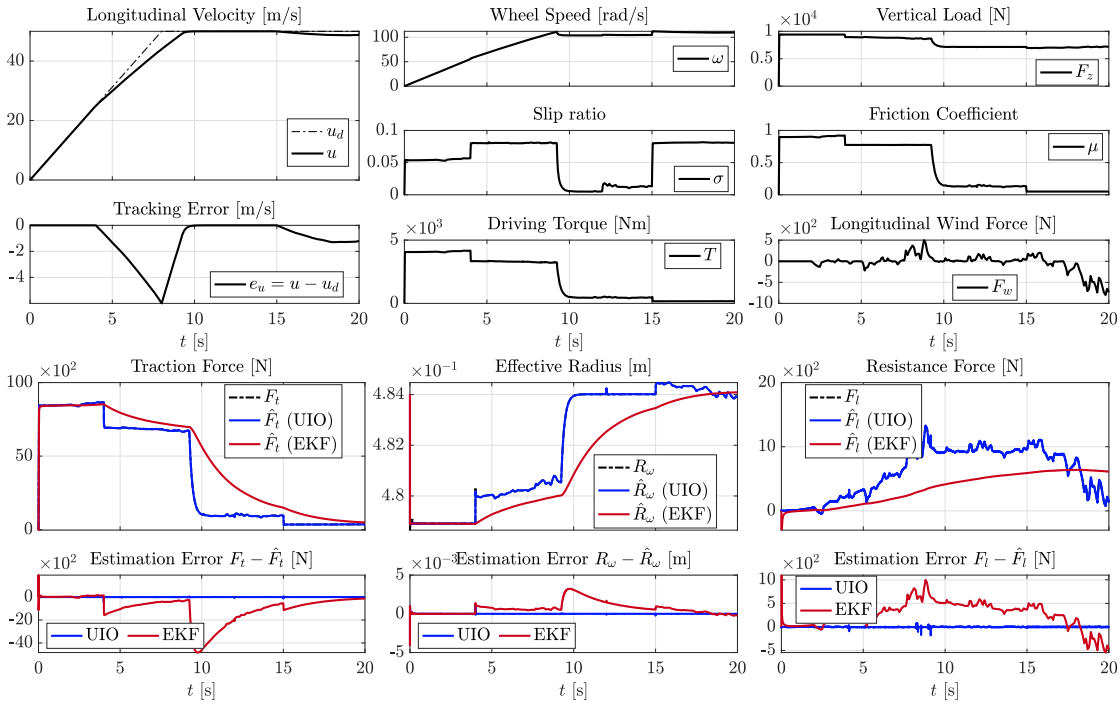

Fig. 4. Scenario #1.2 (Changing Driving Conditions): The racecar is assumed to be traveling along a straight with variable tire-road conditions, switching from dry ($t < 4$) to wet ($4 < t < 12$) to snow ($12 < t < 15$) and finally to ice ($t > 15$). A sudden wind gust is applied at $t = 2$. The proposed estimation and control approach is capable of simultaneously coping with both types of uncertainties and disturbance.

newer measures. Moreover, the performance of a more elaborate EKF, based also on the knowledge of the traction and resistance force models, would not only be dependent on the accuracy of these models and the choice of the covariance matrix, but it would also require a-priori knowledge of the type of tire-road interface, which is unnecessary for the UIO. The second type of simulation run refers to the case where the racecar travels on a straight road with variable tire-road conditions, switching from the dry road, to wet, to snow, and finally to icy road. A sudden wind gust is also considered to show the ability of the method to cope simultaneously with different types of uncertainties. In this case, it is more evident as the proposed UIO is more efficient than the EKF since, the latter, is not able to quickly estimate the sudden changes of tire-road friction. The obtained results are reported in Fig. 4. The scenario of the third simulation is identical to that of the first simulation but with the addition of measurement noise. The results reported in Fig. 5 show as the UIO can estimate the traction force and the other resistance forces to vehicle's motion even in the presence of noise, more effectively than the EKF. It can be observed that, since both the system's states and unknown inputs become state variables of the EKF, the effect of measurement noise on their reconstruction is largely attenuated by the robust property of the filter itself. As a consequence, the estimated signals display only very small fluctuations. This is achieved at the expense of a larger observer's state and a much slower estimation error convergence. Moreover, in the case of the UIO, only the system's states are included as observer variables, and consequently filtered, while the unknown inputs are statically reconstructed by using the formulas in Eq. 20 and 21. Consequently, the state estimates obtained via the UIO have small fluctuations, that are comparable with those of the EKF, while the residual noise, present in such estimates, is directly propagated to the values of estimated unknown inputs. Nonetheless, the estimation error convergence in the UIO is much faster. It is also worth noticing that the proposed controller still guarantees the pursuit of the desired speed profile by committing a negligible tracking error. However, at steady state, small fluctuations of the tracking error can be seen with a maximum absolute value of about 0.02 m/s.

2) Second Simulation Scenario: In this scenario, a simulation was performed by using the Vehicle Dynamics Blockset available for Simulink [59]. The dynamic behavior of the vehicle has been simulated through two sub-blocks: 1) Longitudinal Wheel [60] and 2) Vehicle Body 1DOF Longitudinal [61]. The first allows implementing the longitudinal behavior of an ideal wheel and it is also possible to specify the simulation method of the traction force and the rolling resistance as well as obtaining a series of functional parameters, such as e.g. the torque required for a certain driving cycle. Instead, the second implements a one-degree-of-freedom (1DOF) rigid vehicle with constant mass undergoing longitudinal motion. In this simulation has been reproduced a situation in which the racecar is assumed to be traveling along a straight and dry road, simulated through Pacejka's model, in order to track a longitudinal speed profile $u_d(t)$. The accuracy of the data obtained via the Vehicle Dynamics Blockset is ensured by the use of internal nonlinear models, which are uniformly valid within the car's operating range and whose parameters have been set to the values of common driving conditions. More precisely, the so-called Pacejka's Magic Formula is used, which allows computing the

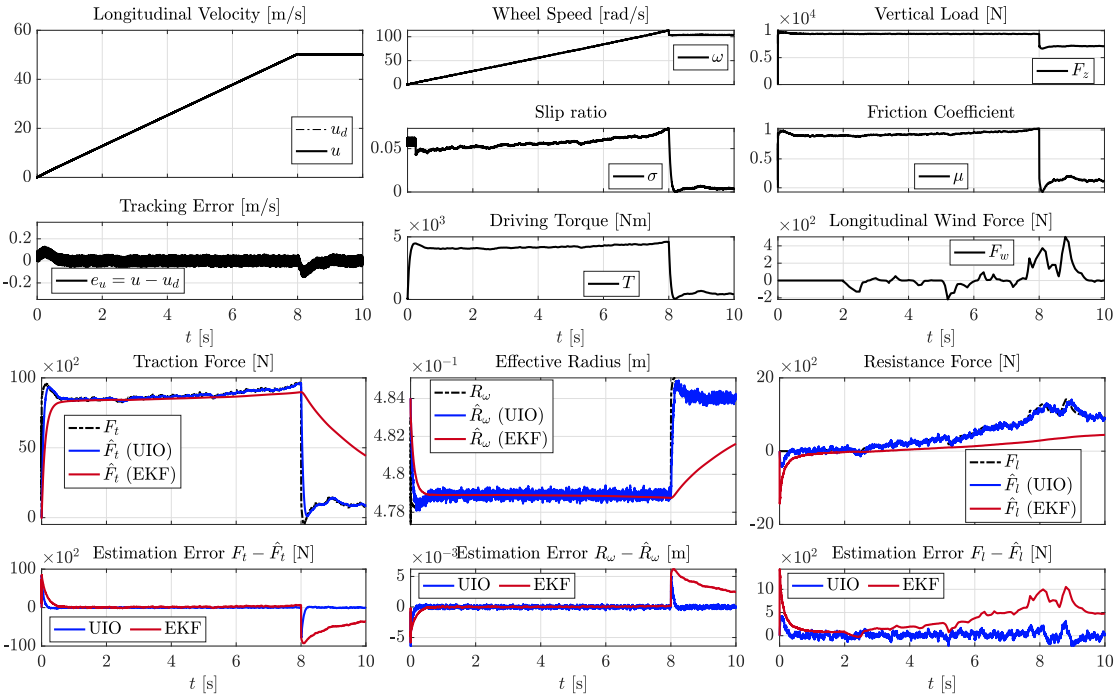

Fig. 5. Scenario #1.3 (Measurements noise): The racecar travels along a straight and dry road and tracks a longitudinal velocity profile $u_d(t)$, when a sudden wind gust hits the vehicle at $t = 2$, in the presence of noise on the measurements. The UIO can reconstruct the unknown inputs and that the controller can track the desired trajectory with a negligible tracking error.

longitudinal traction force F_t according to the empirical four-coefficient expression: $F_t = D\,\sin(C\,\arctan(B\,\sigma - E(B\,\sigma - \arctan(B\,\sigma))))F_z$, where the dimensionless coefficients B, C, D, and E are the stiffness, shape, peak, and curvature of the tire. Their values result from a curve-fitting process of experimental data concerning the different conditions of the tire-asphalt interface [62]. The blockset allows specifying the rolling and aerodynamic coefficients whose values, for the case of racecars, can be found in [63], [64]. The results reported in Fig. 6 show how the controller can follow the desired trajectory with a minimum error and the effectiveness of the disturbance estimation methodology through the UIO, robust compared to the models that can be used to describe the forces of resistance to motion. A small deviation of at most 0.2% of the effective radius reconstructed by the UIO with respect to the one dynamically extracted from the Vehicle Dynamics Blockset can be observed. This is caused by the dynamic deformation of the tire due to speed which is simulated within the block, but it was not considered in the formula of Eq. 20.

3) Simulation of an Aggressive Maneuver as External Process on Raspberry PI: As a final step, the proposed solution involving the input-state estimator of Th. 1 and the longitudinal control law of Th. 2 have been tested by using a low-cost hardware setup, consisting of a Raspberry PI 4 Model B system. This test has been done with the purpose to show the real-time implementability of the solution and assess the required computation time in terms of the CPU utilization. To achieve this, the Matlab/Simulink model, including the full vehicle dynamics modeled via Eq. 1, the estimator, and the control law has been compiled for the Raspberry PI hardware, via the Simulink Real-time Code Generation, and built as a standalone application. The application has been run with a scheduling time $\delta = 10^{-3}$ seconds. The inclusion of the full vehicle model in the simulation represents a further computation load that in an experimental setup would not be necessary. However, this choice allows overestimating the required CPU utilization, further ensuring the solution implementability.

Referring to Fig. 6, the simulated scenario is as follows. The desired longitudinal speed profile is that of an aggressive maneuver, consisting of a fast acceleration phase with $\dot{u}_d = 6.25$ m/s^2 ($t < 7$), a deceleration phase with $\dot{u}_d = -6.25$ m/s^2 ($7 \leq t < 10$), followed another acceleration phase with $\dot{u}_d = 6.25$ m/s^2 till the speed of 50 m/s is reached ($10 \leq t < 15$), and a final constant high-speed motion phase with $\dot{u}_d = 0$ m/s^2 ($15 \leq t < 20$). The road type is dry, except from during the time interval $3 \leq t < 4$ in which the car encounters a wet surface. A Dryden wind blows from the instant $t = 2$ till the end of the simulation. In order to show that the small slip ratio assumption is valid at least within the optimal interval values [26], a larger slip ratio threshold $\bar{\sigma} = 0.17$ has been chosen. While the control law is based on the reduced-degree-of-freedom model, the simulated vehicle dynamics is the full model of Eq. 1, as for the previous simulations.

Analyzing the first row of the figure, one can see the correct functioning of the controller. More precisely, in the phases when the car travels on a dry road, the desired acceleration $\dot{u}_d$ requires a traction force F_t that can be obtained with slip ratio values that are within the allowed range, i.e. $|\sigma| \leq \bar{\sigma}$. During these phases, the controller specifies a correct positive or negative driving torque that allows the asymptotic tracking of the desired speed u_d. As car meets a wet road surface, at $t = 3$, the current traction force F_t instantaneously diminishes, and the asymptotic speed tracking can only be obtained with slip ratios that are out of the allowed range. The controller increases the slip ratio up

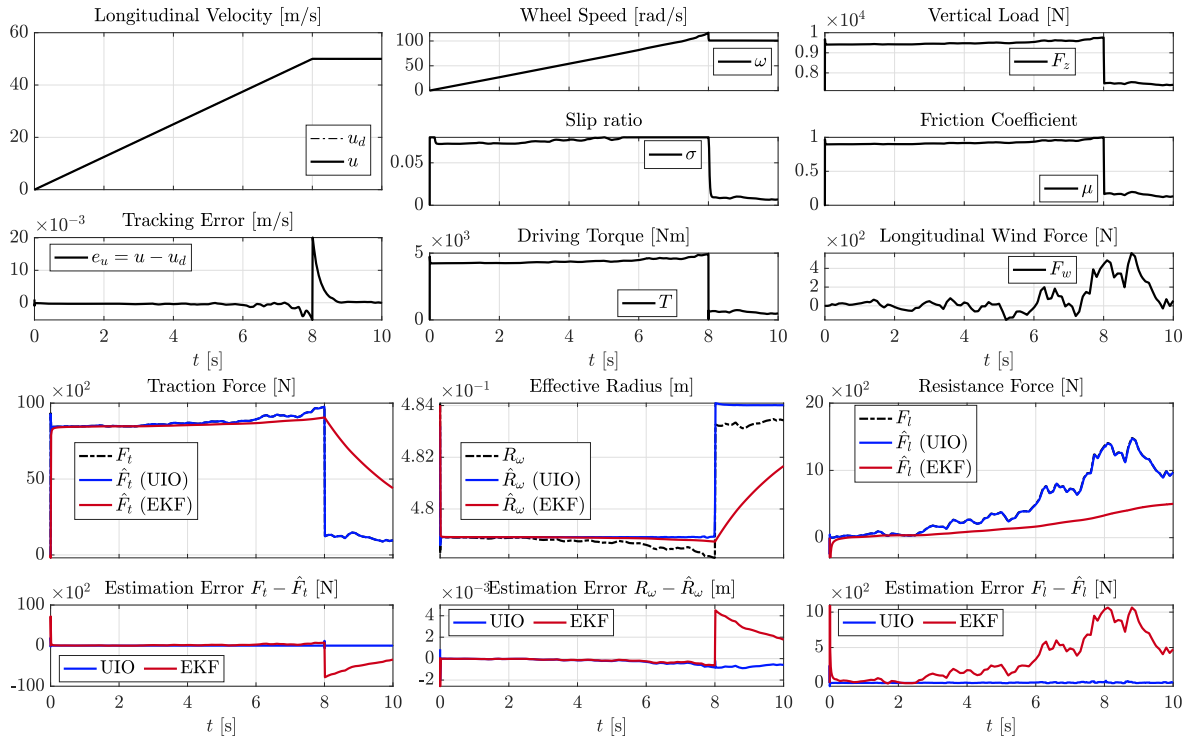

Fig. 6. Scenario #2: (Vehicle Dynamics Blockset with Pacejka's Magic Formula): The proposed UIO estimator and the proposed control are evaluated in a black-box test where the vehicle's dynamics model is simulated via the Vehicle Dynamics Blockset and the traction force is simulated via Pacejka's formula.

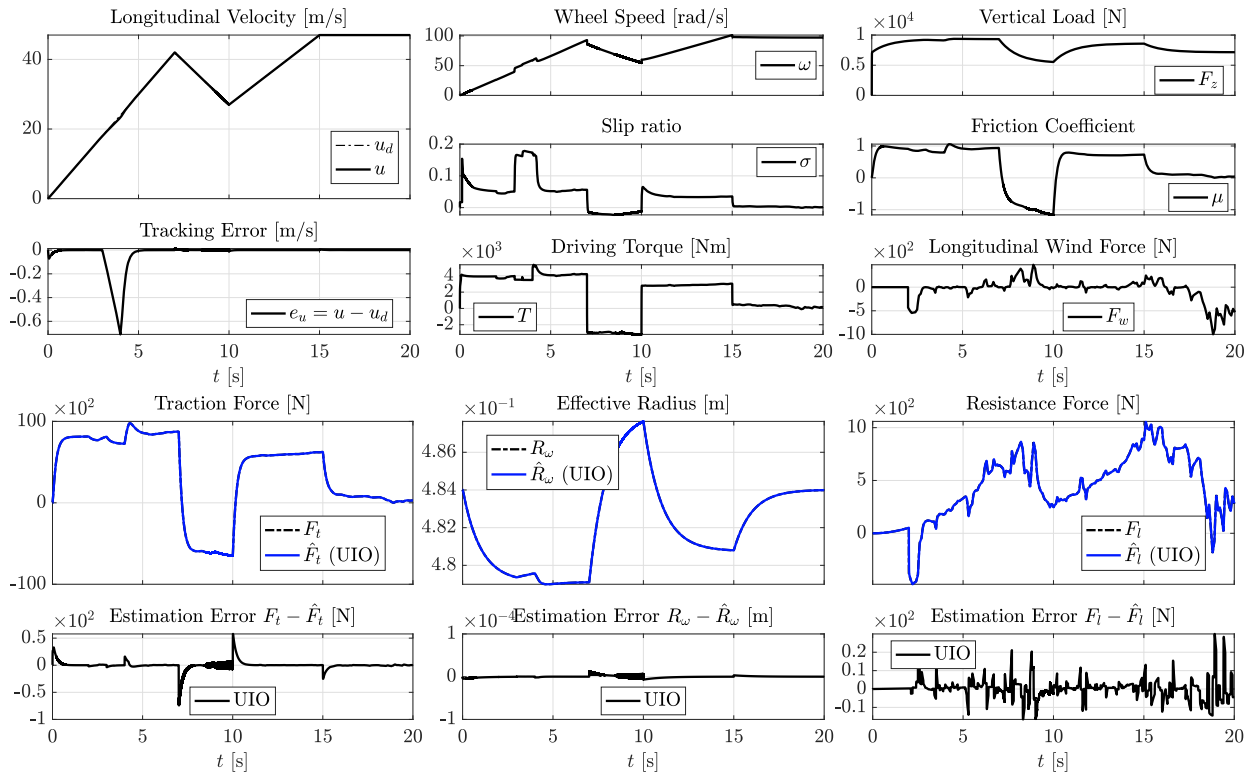

Fig. 7. Scenario #3 (Raspberry PI 4 Model B): Results from the simulation of a complete aggressive maneuver, consisting of fast acceleration, deceleration, and constant high-speed phases, obtained with a standalone process scheduled every $\delta = 10^{-3}$ seconds. The controller successfully allows the asymptotic tracking even with a larger slip ratio threshold $\bar{\sigma} = 0.17$. As the vehicle encounters a wet surface during the interval $t \in [3, 4]$, the controller keeps increasing the longitudinal speed, while maintaining the slip ratio within the allowed range. The estimator correctly and promptly reconstructs the unknown quantities.

TABLE II
ESTIMATION PERFORMANCE ON THE RASPBERRY PI 4 MODEL B

Relative Estim. Error Signal	Average	Standard Dev.
Traction force F_t	$1.356 \cdot 10^{-2}$	$7.823 \cdot 10^{-1}$
Effective tire radius R_ω	$-4.297 \cdot 10^{-9}$	$2.385 \cdot 10^{-6}$
Resistance Force F_l	$1.854 \cdot 10^{-2}$	$1.791 \cdot 10^{-1}$

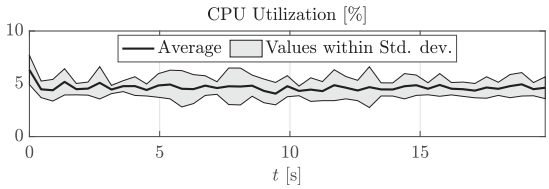

Fig. 8. Scenario #3: Behavior of the CPU utilization percentage, computed on a dataset extracted from 25 runs of the standalone application, including the estimator, the controller, and the full vehicle's dynamics.

to the maximum value and then applies the formula in Eq. 31, in order to make u still increasing, while keeping σ within the allowed range. As the car reaches again a dry surface at $t = 4$ and the required traction force becomes feasible, the tracking speed error quickly converges to zero.

Moving on now to the second row of the figure, it can be seen that also the estimator correctly works, thus providing accurate estimates of the unknown traction force, effective radius, and total resistance force to the controller. Specifically, it can be observed how the effective radius diminishes during the acceleration phases, increases during the deceleration ones, and reaches a constant value when moving at a constant speed. The estimation accuracy has been evaluated in terms of the relative estimation errors and the obtained results have been reported in Table II. Recall that the relative estimation error of a possibly null quantity α estimated by $\hat{\alpha}$ is $|\alpha - \hat{\alpha}| \, (1 + |\alpha|)^{-1}$, where the unity is introduced to cope with the case of $\alpha = 0$.

As a final performance data, the percentage of CPU utilization has been computed by considering 25 runs of the standalone application, including the estimator, the controller, and the full vehicle's dynamics. The obtained results are reported in Fig. 8, which illustrates the behavior of the average of the CPU usage and of the standard deviation. The minimum and maximum utilization values within the standard deviation along the entire simulations is 4.2896% and 5.9606%, respectively, while a typical value is around 4.62%, which shows the practically implementability on the proposed solution even on a low-cost platform.

VI. CONCLUSION

This paper addressed model-free nonlinear control of the longitudinal speed for a self-driving racecar, via the use of a linear UIO allowing the dynamic reconstruction of information on the vehicle's motion concerning the inputs acting on the system. Carried out simulations have highlighted a strong robustness of the proposed estimation and control method to the various simulation models, even in extremely changing conditions, thereby guaranteeing a much safer vehicle's motion than existing techniques. Most prominently, the estimation procedure has proven to be more efficient than EKF-based approaches, even with measurement noise, despite the simplicity of its implementation. Indeed, the approach does not require accurate knowledge of the traction force and all resistance forces. The paper shows that such input uncertainty as well as parametric changes in the corresponding models can be seen as disturbance inputs acting on the system, that can be accurately estimated and compensated. Future work will focus on extending this approach to the complete dynamics of the vehicle and testing it on a real Robocar.

REFERENCES

[1] K. Katsaros and M. Dianati, "Evolution of vehicular communications within the context of 5g systems," *Enabling 5G Commun. Syst. Support Vertical Industries*, pp. 103–126, 2019.
[2] A. Li and K. Luk, "Single-layer wideband end-fire dual-polarized antenna array for device-to-device communication in 5g wireless systems," *IEEE Trans. Veh. Technol.*, vol. 69, no. 5, pp. 5142–5150, May 2020.
[3] T. Hou, Y. Liu, Z. Song, X. Sun, and Y. Chen, "UAV-to-everything (U2X) networks relying on NOMA: A stochastic geometry model," *IEEE Trans. Veh. Technol.*, vol. 69, no. 7, pp. 7558–7568, 2020.
[4] F. Zhu, Z. Li, S. Chen, and G. Xiong, "Parallel transportation management and control system and its applications in building smart cities," *IEEE Trans. Intell. Transp. Syst.*, vol. 17, no. 6, pp. 1576–1585, 2016.
[5] F.-Y. Wang and J. J. Zhang, "Transportation 5.0 in cpss: Towards acp-based society-centered intelligent transportation," in *Proc. 20th IEEE Int. Conf. Intell. Transp. Syst. (ITSC)*, 2017, pp. 762–767.
[6] A. Rucco, G. Notarstefano, and J. Hauser, "An efficient minimum-time trajectory generation strategy for two-track car vehicles," *IEEE Trans. Control Syst. Technol.*, vol. 23, no. 4, pp. 1505–1519, Jul. 2015.
[7] J. Betz *et al.*, "A software architecture for the dynamic path planning of an autonomous racecar at the limits of handling," in *Proc. IEEE Int. Conf. Connected Vehicles and Expo*. IEEE, 2019, pp. 1–8.
[8] A. Heilmeier, A. Wischnewski, L. Hermansdorfer, J. Betz, M. Lienkamp, and B. Lohmann, "Minimum curvature trajectory planning and control for an autonomous race car," *Vehicle Syst. Dyn.*, pp. 1–31, 2019.
[9] Y. Lu, X. Huang, K. Zhang, S. Maharjan, and Y. Zhang, "Blockchain empowered asynchronous federated learning for secure data sharing in internet of vehicles," *IEEE Trans. Veh. Technol.*, vol. 69, no. 4, pp. 4298–4311, Apr. 2020.
[10] R. Singh, D. Saluja, and S. Kumar, "Blind cancellation in radar based self driving vehicles," *IEEE Trans. Veh. Technol.*, vol. 69, no. 7, pp. 6977-6986, Jul. 2020.
[11] Y. Fu, C. Li, R. Yu, T. H. Luan, and Y. Zhang, "A decision-making strategy for vehicle autonomous braking in emergency via deep reinforcement learning," *IEEE Trans. Veh. Technol.*, vol. 69, no. 7, pp. 6977-6986, Jul. 2020.
[12] C. Li, H. Zhang, T. Zhang, J. Rao, L. Y. Wang, and G. Yin, "Cyber-physical scheduling for predictable reliability of inter-vehicle communications," *IEEE Trans. Veh. Technol.*, vol. 69, no. 4, pp. 4192–4206, Jun. 2020.
[13] A. Fagiolini, G. Dini, and A. Bicchi, "Distributed intrusion detection for the security of industrial cooperative robotic systems," *IFAC Proc. Volumes*, vol. 47, no. 3, pp. 7610–7615, 2014.
[14] J. Hu, X. Zhang, and S. Maybank, "Abnormal driving detection with normalized driving behavior data: A deep learning approach," *IEEE Trans. Veh. Technol.*, vol. 69, no. 7, pp. 6943-6951, Jul. 2020.
[15] G. De Nicolao, A. Ferrara, and L. Giacomini, "Onboard sensor-based collision risk assessment to improve pedestrians' safety," *IEEE Trans. Veh. Technol.*, vol. 56, no. 5, pp. 2405–2413, Sep. 2007.
[16] R. Hussain and S. Zeadally, "Autonomous cars: Research results, issues, and future challenges," *IEEE Commun. Surveys Tutorials*, vol. 21, no. 2, pp. 1275–1313, 2018.
[17] D. Caporale *et al.*, "A planning and control system for self-driving racing vehicles," *IEEE 4th Int. Forum Res. Technol. Soc. Ind., RTSI 2018 - Proc.*, 2018.
[18] B. Chen, X. Li, S. A. Evangelou, and R. Lot, "Joint propulsion and cooling energy management of hybrid electric vehicles by optimal control," *IEEE Trans. Veh. Technol.*, vol. 69, no. 5, pp. 4894–4906, May 2020.
[19] L. Ulrich, "Top 10 tech cars: The scramble for electric dominance has begun," *IEEE Spectr.*, vol. 57, no. 4, pp. 30–39, Apr. 2020.
[20] N. A. Greenblatt, "Self-driving cars and the law," *IEEE spectrum*, vol. 53, no. 2, pp. 46–51, 2016.

[21] F. Bohm and K. Häger, "Introduction of autonomous vehicles in the swedish traffic system: Effects and changes due to the new self-driving car technology," Ph.D. dissertation, Univ. Uppsala, 2015.
[22] F. Tian, Y. Yu, X. Yuan, B. Lyu, and G. Gui, "Predicted decoupling for coexistence between wifi and lte in unlicensed band," *IEEE Trans. Veh. Technol.*, vol. 69, no. 4, pp. 4130–4141, Apr. 2020.
[23] E. Awad *et al.*, "The moral machine experiment," *Nature*, vol. 563, no. 7729, pp. 59–64, 2018.
[24] S. Nyholm, "The ethics of crashes with self-driving cars: A roadmap," *Philos. Compass*, vol. 13, no. 7, p. e12507, 2018.
[25] M. Guiggiani, *The Science of Vehicle Dynamics*. Pisa, Italy: Springer Netherlands, 2014.
[26] M. Burckhardt, "Abs und asr, sicherheitsrelevantes, radschlupf-regel system," *Lecture Scriptum, University Braunschweig*, 1987.
[27] H. Pacejka, "Tire and vehicle dynamics," Rotterdam, Netherlands, *Butterworth-Heinemann*, Great Britain, 2012.
[28] S. Watkins, S. Toksoy, and J. Saunders, "On the generation of tunnel turbulence for road vehicles," in *Proc. 11th AFMC*, Hobart, Australia, 1992.
[29] Z. Liang, J. Zhao, Z. Dong, Y. Wang, and Z. Ding, "Torque vectoring and rear-wheel-steering control for vehicle's uncertain slips on soft and slope terrain using sliding mode algorithm," *IEEE Trans. Veh. Technol.*, vol. 69, no. 4, pp. 3805–3815, Apr. 2020.
[30] H. Guo, Z. Yin, D. Cao, H. Chen, and C. Lv, "A review of estimation for vehicle tire-road interactions toward automated driving," *IEEE Trans. Syst., Man, and Cybern.: Syst.*, vol. 49, no. 1, pp. 14–30, Jan. 2019.
[31] C. Diaz *et al.*, "Particle-filtering-based prognostics for the state of maximum power available in lithium-ion batteries at electromobility applications," *IEEE Trans. Veh. Technol.*, vol. 69, no. 7, pp. 7187–7200, Jul. 2020.
[32] C. Huang, L. Li, Y. Liu, and L. Xiao, "Robust observer based intermittent forces estimation for driver intervention identification," *IEEE Trans. Veh. Technol.*, vol. 69, no. 4, pp. 3628–3640, Apr. 2020.
[33] S.-K. Chen, N. Moshchuk, F. Nardi, and J. Ryu, "Vehicle rollover avoidance," *IEEE Control Syst.*, vol. 30, no. 4, pp. 70–85, 2010.
[34] K. Nam, S. Oh, H. Fujimoto, and Y. Hori, "Estimation of sideslip through rls and kalman filter approaches," *IEEE Trans. Ind. Electron.*, vol. 60, no. 3, pp. 988–1000, Mar. 2013.
[35] M. Doumiati, A. Victorino, D. Lechner, G. Baffet, and A. Charara, "Observers for vehicle tyre/road forces estimation: Experimental validation," *Veh. Syst. Dyn.*, vol. 48, no. 11, pp. 1345–1378, 2010.
[36] M. Doumiati, A. Victorino, A. Charara, and D. Lechner, "Onboard real-time estimation of vehicle lateral tire road forces and sideslip angle," *IEEE/ASME Trans. Mechatronics*, vol. 16, no. 4, pp. 601–614, Aug. 2011.
[37] J. Dakhlallah, S. Glaser, S. Mammar, and Y. Sebsadji, "Tire-road forces estimation using extended kalman filter and sideslip angle evaluation," in *Proc. Amer. Control Conf.*, 2008, pp. 4597–4602.
[38] M. Best, T. Gordon, and P. Dixon, "An extended adaptive kalman filter for real-time state estimation of vehicle handling dynamics," *Veh. Syst. Dyn.*, vol. 1, no. 34, pp. 55–75, 2000.
[39] B. Goldfain *et al.*, "Autorally: An open platform for aggressive autonomous driving," *IEEE Control Syst. Mag.*, vol. 39, no. 1, pp. 26–55, Feb. 2019.
[40] S. Sundaram and C. N. Hadjicostis, "Delayed observers for linear systems with unknown inputs," *IEEE Trans. Autom. Control*, vol. 52, no. 2, pp. 334–339, Feb. 2007.
[41] R. Rajamani, "Vehicle Dynamics and Control," Springer Science & Business Media, New York, United States of America, 2011.
[42] H. Guo, R. Yu, W. Qiang, and H. Chen, "Optimal slip based traction control for electric vehicles using feedback linearization," in *Proc. IEEE Int. Conf. Mechatron. Control*, 2014, pp. 1159–1164.
[43] O. Walter, J. Schmalenstroeer, A. Engler, and R. Haeb-Umbach, "Smartphone-based sensor fusion for improved vehicular navigation," in *Proc. 10th IEEE Workshop Positioning, Navigation and Commun.*, 2013, pp. 1–6.
[44] F. Massa, L. Bonamini, A. Settimi, L. Pallottino, and D. Caporale, "Lidar-based gnss denied localization for autonomous racing cars," *Sensors*, vol. 20, no. 14, p. 3992, 2020.
[45] R. No, "Regulation no 39 of the economic commission for europe of the united nations (un/ece), uniform provisions concerning the approval of vehicles with regard to the speedometer equipment including its installation," Official Journal of the European Union, vol. 120, pp. 40–48, 2010. [Online]. Available. https://eur-lex.europa.eu/LexUriServ/LexUriServ.do?uri=OJ:L:2010:120:0040:0048:EN:PDF
[46] K. A. Al-Gaadi, "Testing the accuracy of autonomous gps in ground speed measurement," *J. Appl. Sci*, vol. 5, pp. 1518–1522, 2005.
[47] M. Sain and J. Massey, "Invertibility of linear time-invariant dynamical systems," *IEEE Trans. Aut. Control*, vol. 14, no. 2, pp. 141–149, Apr. 1969.
[48] M. Hou and R. J. Patton, "Input observability and input reconstruction," *Automatica*, vol. 34, no. 6, pp. 789–794, 1998.
[49] S. Sundaram, "Lecture notes in fault-tolerant and secure control systems," University of Waterloo, Canada, 2011.
[50] R. N. Jazar, "Driveline dynamics," in *Vehicle Dynamics*. Melbourne, Australia, Springer, 2017, pp. 173–223.
[51] G. Welch and G. Bishop, "An introduction to the kalman filter," *University North Carolina at Chapel Hill*, 2006.
[52] L. Biagiotti, "State estimation in presence of disturbances: The Kalman filter," *Lectures Slided Control Syst. Theory*, University of Modena and Reggio Emilia, Italy, 2016. [Online]. Available. http://www.dii.unimore.it/~lbiagiotti/MaterialeTSC1516/TSC-03-KalmanFilter.pdf
[53] S. G. Mohinder and A. P. Andrews, "Kalman filtering, theory and practice using matlab, third edition," *WILEY*, 2008.
[54] F. Naets, S. Van Aalst, B. Boulkroune, N. El Ghouti, and W. Desmet, "Design and experimental validation of a stable two-stage estimator for automotive sideslip angle and tire parameters," *IEEE Trans. Veh. Technol.*, vol. 66, no. 11, pp. 9727–9742, 2017.
[55] M. Dousti, S. C. Baslamısli, E. T. Onder, and S. Solmaz, "Design of a multiple-model switching controller for abs braking dynamics," *Trans. Inst. Meas. and Control*, vol. 37, no. 5, pp. 582–595, 2015.
[56] A. Ružinskas and H. Sivilevičius, "Magic formula tyre model application for a tyre-ice interaction," *Procedia Eng*, vol. 187, pp. 335–341, 2017.
[57] T. M. I. Hakim and O. Arifianto, "Implementation of drydend continuous turbulence model into simulink for LSA-02 flight test simulation," in *Proc. 5th Int. Semin. Aerosp. Sci. Technol.*, 2018, pp. 1–12.
[58] Dryden wind turbulence model. [Online]. Available: https://it.mathworks.com/help/ aeroblks/drydenwindturbulencemodelcontinuous.html
[59] Vehicle dynamics blockset, 2018. [Online]. Available: https://it.mathworks.com/products/vehicle-dynamics.html#full- vehicle. Accessed on: Aug. 8, 2020.
[60] Longitudinal wheel, 2018. [Online]. Available: https://it.mathworks.com/help/autoblks/ref/longitudinalwheel.html. Accessed on: Jun. 1, 2020
[61] Vehicle body 1dof longitudinal, 2018. [Online]. Available: https://it.mathworks.com/help/autoblks/ref/vehiclebody1doflongitudinal. % html. Accessed on: Apr. 23, 2020.
[62] L. Li, F.-Y. Wang, and Q. Zhou, "Integrated longitudinal and lateral tire/road friction modeling and monitoring for vehicle motion control," *IEEE Trans. Intell. Transp. Syst.*, vol. 7, no. 1, pp. 1–19, Mar. 2006.
[63] J. Katz, *Race Car Aerodynamics*. San Diego (CA), United States of America. Bentley Publishers, United States, 2006.
[64] G. Genta, *Motor Vehicle Dynamics*. Torino, Italy. Series on Advances in Mathematics for Applied Sciences, World Scientific, Singapore, vol. 43, 2006.

Salvatore Pedone received the M.S. degree in aerospace engineering, in 2018 from the University of Palermo, Palermo, Italy, where he is currently working toward the Ph.D. degree in information, communication, and technology. His research interests focus on the development of control and estimation systems for self-driving vehicles and UAVs.

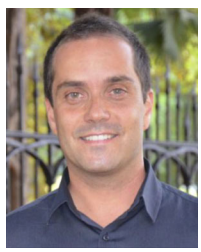

Adriano Fagiolini received the M.S. degree in computer science engineering and the Ph.D. degree in robotics and automation from the University of Pisa, Pisa, Italy, in 2004 and 2009, respectively. He is currently an Assistant Professor with the University of Palermo, Palermo, Italy. He has been a Visiting Researcher with the Department of Energy, IUT Longwy Université de Lorraine, France, in 2019, and with the Department of Mechanical Engineering, University of California at Riverside, in 2015 and 2017. He enrolled in the Summer Student Programme with the European Center for Nuclear Research (CERN), Geneva, in 2002. In 2008, he led the team of the University of Pisa during the first European Space Agency's Lunar Robotics Challenge, which resulted in a second-place prize for the team. He was one of the recipients of the IEEE ICRA's Best Manipulation Paper Award in 2005.